

Clinical Radiosynthesis and Translation of [¹⁸F]OP-801: A Novel Radiotracer for Imaging Reactive Microglia and Macrophages

Isaac M. Jackson, Mackenzie L. Carlson, Corinne Beinat, Noeen Malik, Mausam Kalita, Samantha Reyes, E. Carmen Azevedo, Sydney C. Nagy, Israt S. Alam, Rishi Sharma, Santiago Appiani La Rosa, Farshad Moradi, Jeffrey Cleland, Bin Shen, and Michelle L. James*



Cite This: <https://doi.org/10.1021/acschemneuro.3c00028>



Read Online

ACCESS |



Metrics & More



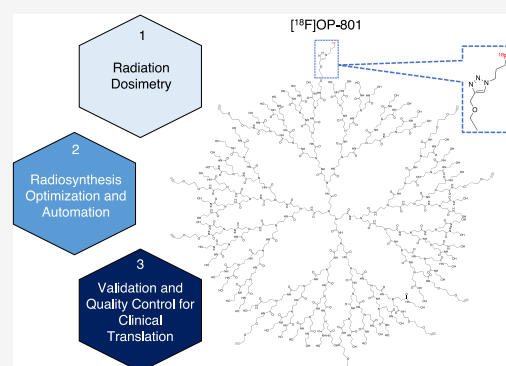
Article Recommendations



Supporting Information

ABSTRACT: Positron emission tomography (PET) is a powerful tool for studying neuroinflammatory diseases; however, current PET biomarkers of neuroinflammation possess significant limitations. We recently reported a promising dendrimer PET tracer ([¹⁸F]OP-801), which is selectively taken up by reactive microglia and macrophages. Here, we describe further important characterization of [¹⁸F]OP-801 in addition to optimization and validation of a two-step clinical radiosynthesis. [¹⁸F]OP-801 was found to be stable in human plasma for 90 min post incubation, and human dose estimates were calculated for 24 organs of interest; kidneys and urinary bladder wall without bladder voiding were identified as receiving the highest absorbed dose. Following optimization detailed herein, automated radiosynthesis and quality control (QC) analyses of [¹⁸F]OP-801 were performed in triplicate in suitable radiochemical yield ($6.89 \pm 2.23\%$ decay corrected), specific activity (37.49 ± 15.49 GBq/mg), and radiochemical purity for clinical imaging. Importantly, imaging mice with tracer (prepared using optimized methods) 24 h following the intraperitoneal injection of liposaccharide resulted in the robust brain PET signal. Cumulatively, these data enable clinical translation of [¹⁸F]OP-801 for imaging reactive microglia and macrophages in humans. Data from three validation runs of the clinical manufacturing and QC were submitted to the Food and Drug Administration (FDA) as part of a Drug Master File (DMF). Subsequent FDA approval to proceed was obtained, and a phase 1/2 clinical trial (NCT05395624) for first-in-human imaging in healthy controls and patients with amyotrophic lateral sclerosis is underway.

KEYWORDS: positron emission tomography, F-18, click chemistry, dendrimer, clinical translation, neuroinflammation



1. INTRODUCTION

Innate immune responses in the central nervous system (CNS) can be both helpful and harmful. Involving activation of central (microglia) and peripheral (macrophages) cells in addition to the generation and release of cytokines and chemokines, long-term aberrant innate immune activation has been linked to several neurological diseases including amyotrophic lateral sclerosis (ALS), multiple sclerosis, and Alzheimer's disease.^{1,2} Unfortunately, the high complexity and dynamic nature of innate immune processes in different disease types/stages, and the lack of effective tools to accurately study these processes, has resulted in sizeable knowledge gaps regarding the *in vivo* spatiotemporal dynamics of these cells in different patient populations. Accordingly, considerable efforts are being made to better understand the immune response to improve diagnosis, monitoring, and treatment of neurological disease. Notably, there is currently no single technique that enables truly specific and sensitive detection of activated microglia and macrophages and their associated function in the clinical setting.

The high sensitivity and minimally invasive nature of positron emission tomography (PET) make this imaging modality an attractive tool for longitudinally studying molecular processes such as neuroinflammation *in vivo*. Unfortunately, current PET biomarkers for neuroinflammation possess notable limitations. The most widely evaluated neuroinflammation PET biomarker, translocator protein 18 kDa (TSPO), has helped establish the immense potential of neuroinflammation PET but faces significant limitations: the functional relevance of TSPO in diseases of interest is unclear, and non-specific expression across many cell types complicates image analysis and confounds interpretation of clinical data.^{3,4} While alternative biomarkers (*e.g.*, P2X ligand-gated ion

Received: January 13, 2023

Accepted: May 22, 2023

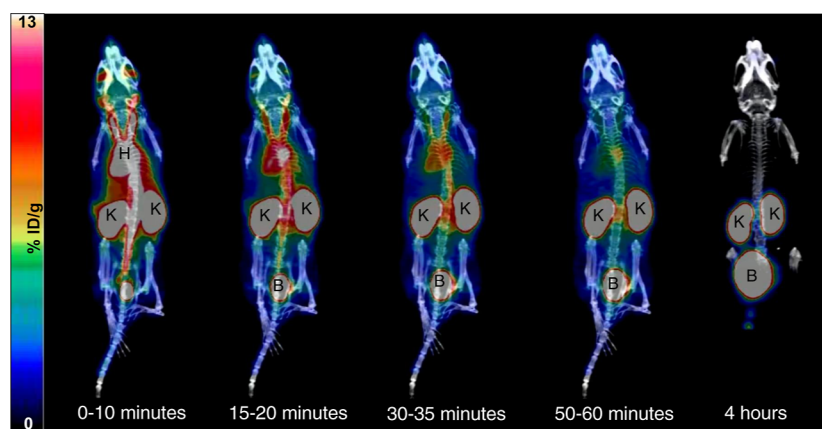


Figure 1. Representative PET images from a subset of dosimetry timepoints in healthy naïve female mice. Regions of interest were drawn around key organs, with kidney and bladder representing areas with the highest uptake (B = bladder, K = kidney, and H = heart).

channel type 7 [P2X7R] and colony-stimulating receptor factor 1 [CSF1R]) are currently under investigation, they and/or their corresponding tracers are likewise limited by numerous factors including target expression across multiple cell types, poor blood–brain barrier (BBB) permeability, and/or high non-specific binding.^{5,6}

Dendrimers are synthetic nanoparticles with highly ordered branching surfaces and tuneable properties (*e.g.*, structurally modifiable terminal endings and controlled size) that offer a potential solution to current limitations of many neuroinflammation PET tracers.^{7,8} *In vivo* behavior (*i.e.*, distribution, clearance, and CNS uptake) has been demonstrated to be contingent on modifiable properties including size, charge, and functional groups. Studies with fluorescently labeled fourth generation polyamidoamine (PAMAM) hydroxyl dendrimers have shown that while these compounds do not cross the healthy intact BBB, they do cross the BBB in the context of inflammation, adequately diffuse through brain parenchyma, and are taken up by reactive microglia and macrophages in a rapid and highly specific manner *via* fluid phase endocytosis.^{7,22} Moreover, these dendrimers have a high signal-to-background ratio due to their quick clearance from regions not containing rapidly endocytosing myeloid cells and are amenable to radiolabeling.^{4–9} Although several dendrimer-based PET tracers have been reported previously (*e.g.*, a ⁶⁴Cu-labeled LyP-1-dendrimer and a ¹⁸F-labeled synthetic dendron [half-dendrimer] for PET imaging of atherosclerotic plaques and HER2 expressing cells, respectively, and a ^{99m}Tc-labeled dendrimer for single photon emission computed tomography imaging of apoptotic cancer cells), none of these specifically target reactive immune cells in the context of neuroinflammation.^{10–13}

We recently described the initial radiosynthesis and preclinical evaluation of a generation 4 PAMAM hydroxyl dendrimer PET tracer, [¹⁸F]OP-801, that is known to be selectively taken up (>95%) by activated microglia and macrophages, predominantly *via* fluid phase endocytosis.^{14–16} This tracer has shown tremendous promise preclinically, displaying *in vivo* whole brain uptake that increases linearly with severity of sepsis-induced inflammation in a lipopolysaccharide (LPS) mouse model. Specifically, we found significantly elevated [¹⁸F]OP-801 signal in the cortex, medulla, olfactory bulb, and pons of LPS mice—regions that correspond with the presence of reactive microglia and macrophages in this model.¹⁴ We also demonstrated the utility

of ¹⁸F-OP-801 for detecting neuroinflammation in the spinal cord in an experimental autoimmune encephalomyelitis (EAE) mouse model with high sensitivity and specificity and demonstrated that this tracer can monitor response to a novel CSF1R inhibitor in the EAE mouse model.¹⁷ Cumulatively, these preclinical imaging results in murine disease models highlight the promise of [¹⁸F]OP-801 PET as a sensitive and specific imaging technique to quantify and track innate immune function in multiple CNS diseases, thus motivating us to translate this agent to the clinic.

Here, we report critical data regarding the characterization of [¹⁸F]OP-801 for clinical translation, including radiation dosimetry studies to establish safe dose limits in humans and stability studies. Moreover, a single intravenous good laboratory practice (GLP) dose toxicology study was conducted in rats and used in conjunction with human micro-dosing guidelines (as per ICH topic M3 [R2])¹⁸ and direct, specific feedback from the FDA to guide optimization, automation, and validation of [¹⁸F]OP-801 radiosynthesis in yields and molar activity suitable for clinical use. The studies described herein afforded definitive data to facilitate clinical translation and reliable radiosynthesis of [¹⁸F]OP-801 for imaging neuroinflammation in humans.

2. RESULTS AND DISCUSSION

2.1. Dosimetry, *In Vitro* Plasma Stability, and Toxicology Studies. Dosimetry studies for [¹⁸F]OP-801 in mice were performed using both biodistribution (Supporting Information) and image-analysis based methods (Figure 1). To estimate dosimetry in humans, we applied data from image analysis-based dosimetry studies in male and female mice. Recent work has demonstrated image-based methods to be reliable for computing dose estimates, with a number of benefits compared to traditional biodistribution-based methods.^{19,20} Image-based estimation allows for collection of longitudinal data from the same animals, despite being limited by technical difficulty of segmenting small organs. The PET system used in these studies can deliver 1.5 mm spatial resolution at the center of the 12.7 mm field of view, meaning that smaller volumes of interest (VOIs) such as lymph nodes were not included in the image-based analysis due to limitations in resolution. Importantly, these smaller VOIs (*e.g.*, lymph nodes) do not encompass heavily contributive source organs to radiation dose or affect dose limits in mice or humans.

Based on murine imaging data, absorbed doses were quantified for 24 organs of interest and used to predict human dosimetry (Table 1). Since the highest doses were

Table 1. Image-Based Estimated Radiation Dose to Human Adults after IV Injection of [¹⁸F]OP-801

organ	female (mSv/MBq)	male (mSv/MBq)
adrenals	1.68×10^{-3}	2.06×10^{-3}
brain	4.55×10^{-4}	7.82×10^{-4}
breasts	2.78×10^{-4}	3.73×10^{-4}
gallbladder wall	1.14×10^{-3}	1.52×10^{-3}
LLI wall	1.70×10^{-3}	8.23×10^{-4}
small intestine	1.14×10^{-3}	9.24×10^{-4}
stomach wall	6.94×10^{-4}	9.70×10^{-4}
ULI wall	9.84×10^{-4}	9.12×10^{-4}
heart wall	1.66×10^{-3}	1.76×10^{-3}
kidneys	3.15×10^{-2}	4.52×10^{-2}
liver	2.45×10^{-3}	2.68×10^{-3}
lungs	2.64×10^{-3}	2.79×10^{-3}
muscle	1.15×10^{-3}	1.37×10^{-3}
ovaries	1.72×10^{-3}	
pancreas	1.19×10^{-3}	1.62×10^{-3}
red marrow	7.51×10^{-4}	8.38×10^{-4}
osteogenic cells	5.17×10^{-4}	6.55×10^{-4}
skin	3.35×10^{-4}	4.01×10^{-4}
spleen	1.32×10^{-3}	1.73×10^{-3}
thymus	4.41×10^{-4}	6.55×10^{-4}
thyroid	2.18×10^{-4}	4.85×10^{-4}
urinary bladder wall	5.34×10^{-2}	9.00×10^{-3}
uterus	3.10×10^{-3}	1.17×10^{-3}
total body	1.05×10^{-3}	1.21×10^{-3}
testes		5.54×10^{-4}
effective dose	4.08×10^{-3}	2.62×10^{-3}

detected in the kidneys and urinary bladder wall, these are predicted to be the dose-limiting organs in humans, with an average of 0.031 and 0.045 mSv/MBq in the kidneys and 0.053 and 0.090 mSv/MBq in the urinary bladder wall for human females and males, respectively (Table 1). The radiation dose generally regarded as safe (GRAS) for an adult human research subject is 3 Rem/single dose (5 Rem/year) to the whole body, active blood-forming organs, lens of the eye, and gonads and 5 Rem/single dose (15 Rem/year) for the other organs, ultimately translating to a maximum GRAS [¹⁸F]OP-801 administered activity of 1587.3 MBq per scan (4761.9 MBq per year) for females and 1106.3 MBq per scan (3318.53 MBq per year) for males.²¹ Importantly, these maximum allowed activities are considerably higher than the average administered activity of a F-18 PET tracer administered for clinical imaging (approx. 300 MBq), which supports longitudinal clinical imaging with [¹⁸F]OP-801 as a biomarker for tracking neuroinflammation. Notably, these dosimetry estimates were calculated using the most conservative approach by assuming decay of administered dose within the organ. While the urinary bladder wall was found to be the dose-limiting organ based on image analysis in female mice, this dose is likely to be lower in

a clinical setting where voiding will be encouraged as part of the clinical imaging protocol to reduce dose in this tissue. Consequently, we predict that the most accurate dose-limiting organ will be the kidney.

Importantly, image-based dosimetry calculations also help predict the mechanism of clearance for radiotracers. Prior to PET imaging studies with [¹⁸F]OP-801, extensive studies of generation 4 PAMAM hydroxyl dendrimers and fluorescent analogues have established that these molecules are predominantly and rapidly cleared renally in rabbits, canines, and rats.^{22–24} Our estimates from mouse PET image analyses are congruent with these previous observations (Table 2). To thoroughly characterize [¹⁸F]OP-801 and predict tracer uptake and distribution in humans, we also showed that [¹⁸F]OP-801 is stable in human plasma at 37 °C; on analytical high-performance liquid chromatography (HPLC), we observed 100% intact parent tracer with no appearance of radio-metabolite peaks for up to 90 min of incubation (Supporting Information Figure 3).

In anticipation of clinical translation, we conducted a single intravenous GLP dose toxicology study of [¹⁹F]OP-801 in rats to establish a No-Observed-Adverse-Event-Level (NOAEL) compatible with human micro-dosing of [¹⁹F]OP-801 (defined as 100 μg mass per dose, as described in IHC topic M3 [R2]).¹⁸ Briefly, mice were administered [¹⁹F]OP-801, and clinical and pathological assessments were performed up to 14 days post-dose (see the Supporting Information for details on study design and results). Importantly, no adverse effects were seen at this dose. All animals survived to scheduled date of sacrifice for post-mortem analysis (2 or 13 days, respectively) without any major findings observed. A NOAEL was established as 4.7 mg/kg/day (the highest dose tested), supporting a greater than 3000-fold safety factor for the proposed human dose. Cumulatively, these results, combined with our published and ongoing preclinical findings, are very encouraging and helped guide the optimization of [¹⁸F]OP-801 synthesis for clinical translation.

2.2. Radiosynthesis Method Optimization. The overarching approach for clinical synthesis was planned to be very similar to that previously described for preclinical synthesis. Briefly, [¹⁸F]3-Fluoropropylazide was accessed *via* nucleophilic fluorination of a tosyl precursor, purified *via* HPLC, trapped and eluted from a Sep-Pak, and subsequently reacted with the PAMAM-G4-OH alkyne₁₀ dendrimer precursor *via* CuAAC click chemistry to yield [¹⁸F]OP-801. The tracer was purified by HPLC and reformulated to furnish [¹⁸F]OP-801 suitable for the injection (Figure 2). A key consideration guiding synthetic optimization was a 100 μg per dose mass limit based on human micro-dosing guidelines per ICH topic M3 (R2)¹⁸ as well as direct pre-submission feedback from the FDA regarding development of [¹⁸F]OP-801. Adhering to this cutoff allowed for submission to the FDA with toxicology data in a single species, per ICH topic M3 (R2),¹⁸ potentially facilitating rapid translation and evaluation in humans prior to further methodology work or potential optimization. Subsequently, considerable synthetic optimization was required to ensure

Table 2. Image-Based Estimates for AUC in Human Males and Females

	bladder	bone	brain	heart	kidney	liver	lung	muscle
male (image)	0.01791	0.00075	0.00410	0.00466	0.07357	0.01445	0.01309	0.13922
female (image)	0.08648	0.00024	0.00223	0.00439	0.05009	0.01119	0.01039	0.05054

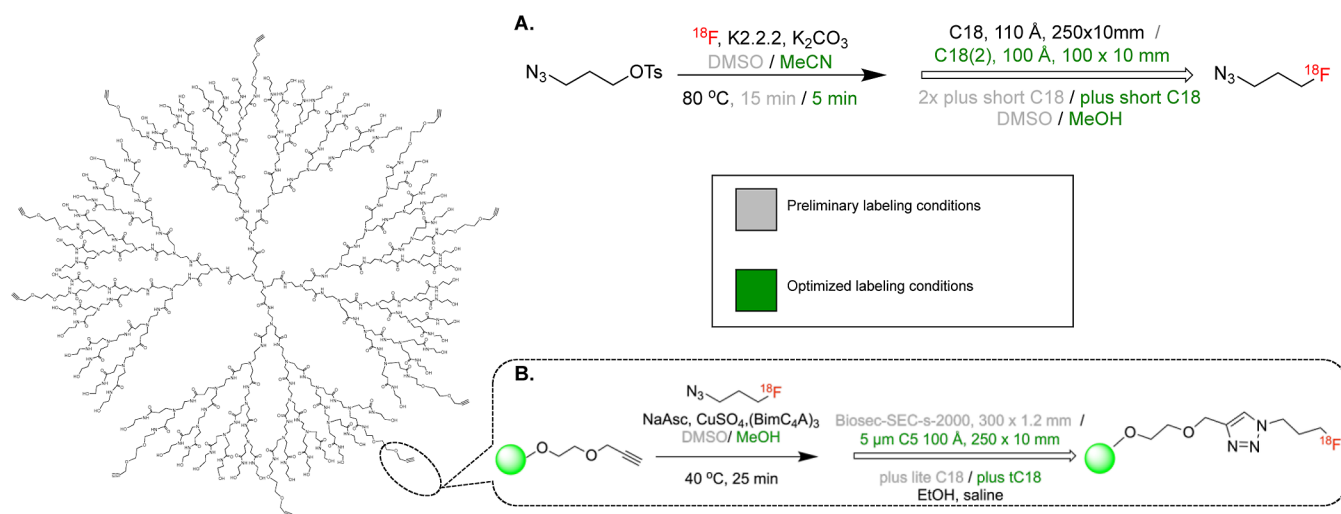


Figure 2. Radiosynthesis of $[^{18}\text{F}]$ OP-801 was achieved in two steps: (A) nucleophilic $[^{18}\text{F}]$ fluorination of a tosyl precursor yielded $[^{18}\text{F}]$ 3-fluoropropylazide. (B) Alkyne dendrimer precursor was reacted with $[^{18}\text{F}]$ 3-fluoro-propylazide via copper-catalyzed azide–alkyne cycloaddition and reformulated to provide $[^{18}\text{F}]$ OP-801 suitable for clinical use.

that we could efficiently and reproducibly manufacture doses within this target 100 μg per dose mass limit.

Notably, gross similarities in size and other relevant properties mean that the radiolabeled $[^{18}\text{F}]$ OP-801 and the PAMAM-G4-OH alkyne₁₀ dendrimer precursor cannot be resolved by semi-preparative HPLC. In light of this, in conjunction with the constraints imposed by working with radioactivity and the relatively short half-life of fluorine-18 (110 min), we determined that the most efficient and reproducible way to meet these mass limits was to establish a synthetic route that could reproducibly yield high specific activity (SA) $[^{18}\text{F}]$ OP-801 from a starting PAMAM-G4-OH alkyne₁₀ dendrimer precursor mass of 100 μg (Figure 2). By ensuring the cumulative non-radioactive mass of tracer and unlabeled precursor in a batch would be 100 μg or less, this approach guarantees that individual doses will be within the micro-dosing limits described in ICH topic M3 (R2).¹⁸ Importantly, this reduces the likelihood of clinical doses failing quality control (QC) due to low SA and high non-radioactive mass. This starting mass of 100 μg is substantially less than the starting precursor mass for the most automated radiosynthetic methods (*i.e.*, ≥ 1 mg), including preclinical synthesis of $[^{18}\text{F}]$ OP-801 (*i.e.*, 3–5 mg),¹⁴ which in turn warranted significant methodology studies and synthesis optimization of both steps prior to translation.

We found the CuAAC step to be highly sensitive to reaction stoichiometry, particularly depending on starting mass of the alkyne precursor, total reaction volume, and amount of $[^{18}\text{F}]$ 3-fluoropropylazide available for the reaction. Holding all other conditions constant, CuAAC conversion of $[^{18}\text{F}]$ 3-fluoropropylazide to $[^{18}\text{F}]$ OP-801 was directly proportional to the concentration of the PAMAM-G4-OH alkyne₁₀ dendrimer precursor present in solution and inversely proportional to the starting mass of the alkyne precursor. Accordingly, holding all other conditions constant, starting precursor mass of less than 0.5 mg began to show decreases in CuAAC yield (Supporting Information Figure 4). Given that starting alkyne precursor mass was fixed based on toxicology studies, this demanded a robust means of synthesizing and isolating (radio-)chemically pure $[^{18}\text{F}]$ 3-fluoropropylazide in a small volume with a high yield.

Key factors to increase yield and purity of $[^{18}\text{F}]$ 3-fluoropropylazide included reducing thermolysis by decreasing reaction time and changing HPLC and Sep-Pak conditions for purification and trapping (Figure 2A). To minimize the elimination and hydrolysis byproducts, we reduced reaction time for the fluorination step and pursued a combination HPLC and cartridge exchange approach for isolation of this key intermediate. Although fluoro-azides for ^{18}F click chemistry are often isolated through distillation, concern for volatile byproducts and impurities that could ultimately lead to inconsistently reproducible radiolabeling in the click chemistry step motivated us to pursue an HPLC/cartridge-based approach to purification and reformulation.

$[^{18}\text{F}]$ 3-fluoropropylazide was found to be significantly hydrophilic; consequently, the trapping efficiency on a Sep-Pak was inversely proportional to both total volume of the collected HPLC eluent, as well as % MeCN in the eluent (Supporting Information Figure 5). Optimizing for low total volume and % MeCN was achieved by diluting the crude product with acid prior to the injection onto HPLC and changing HPLC conditions, which cumulatively served to improve the peak shape and shorten the retention time. Under optimized Sep-Pak trapping conditions, the elution efficiency of $[^{18}\text{F}]$ 3-fluoropropylazide with 1 mL of MeOH was $83 \pm 3\%$ ($n = 8$). Methanol was selected as the eluent due to its common use as a CuAAC solvent, eliminating the need for an evaporation step with potential for volatilization of the low-molecular-weight azide intermediate between reaction steps. Under these conditions, the maximum CuAAC yield with 0.1 mg of the alkyne dendrimer precursor was approximately 83% from $[^{18}\text{F}]$ 3-fluoropropylazide (Supporting Information Figure 4).

2.3. Assessment of PET Image Quality Using Clinical Grade $[^{18}\text{F}]$ OP-801 in a Mouse Model of Neuroinflammation. Although radiolabeled $[^{18}\text{F}]$ OP-801 and the PAMAM-G4-OH alkyne₁₀ dendrimer precursor cannot be resolved by semi-preparative HPLC due to gross similarities in size and other relevant properties, we hypothesized that the presence of unlabeled dendrimer precursors, and more broadly SA, will not have a significant effect on uptake and distribution because the tracer is taken up by fluid phase endocytosis, as

opposed to competitive receptor binding. To confirm this hypothesis and rule out any differences in the uptake and distribution of [^{18}F]OP-801 due to changes in the injected mass (when comparing our standard preclinical tracer synthesis method to that of our optimized clinical synthesis method), we compared brain PET images of LPS-injected mice acquired using the optimized clinical (low PAMAM-G4-OH alkyne₁₀ dendrimer precursor starting mass) [^{18}F]OP-801 synthesis protocol to images acquired following the injection of the tracer made using the preclinical (high precursor starting mass) synthetic route (Figure 3).

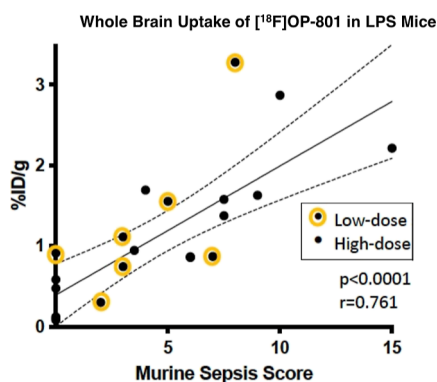


Figure 3. Whole brain uptake of [^{18}F]OP-801 (% ID/g) was plotted against the murine sepsis score for two sets of murine LPS imaging studies performed with the tracer synthesized via the preclinical high-mass and clinically validated low-mass protocols, respectively. Line is fit to all datapoints and shows high correlation between whole brain uptake and sepsis score, with no differences seen between synthetic routes or associated mass dose of the tracer.¹⁴

SA and injected non-radioactive mass of [^{18}F]OP-801 per dose were compared for mice with LPS-induced sepsis using

these two respective protocols. Average non-radioactive mass and average SA were found to be markedly lower for doses prepared with the optimized clinical (low mass) synthetic route ($n = 3$, starting alkyne precursor mass 0.1 mg, avg. mass per dose = 0.42 μg , SD 0.15) than that for those prepared with the preclinical (high mass) synthetic route ($n = 3$, starting alkyne precursor mass 3–5 mg, avg. mass per dose = 4.30 μg , SD 3.35) (Supporting Information Table 3). Accordingly, SA was significantly higher for optimized low mass syntheses (average SA = 10.18 GBq/mg, SD 2.78) relative to the preclinical high mass synthetic route (average SA = 1.87 GBq/mg, SD 1.48). We conducted PET imaging studies of mice 24 h after receiving an intraperitoneal injection of LPS (10 mg/kg) using our previously described methods,¹⁴ with tracer doses prepared via both methods. Importantly, whole brain uptake of [^{18}F]OP-801 in mice with varying murine sepsis scores (levels of severity) was consistent across synthesis conditions: the slope did not differ significantly by adding low mass results ($n = 7$ mice) to high mass results ($n = 15$ mice), and linear correlation between score and whole brain uptake remained significant and positive (high mass synthesis only $p < 0.0001$, $r = 0.854$, combined $p < 0.0001$, $r = 0.761$; Figure 3).

2.4. Automated Radiosynthesis, Validation, and QC for Clinical Production. We applied our optimized radiochemistry under Good Manufacturing Process (cGMP) guidelines to conduct clinical grade [^{18}F]OP-801 validation runs and complete Chemistry, Manufacturing, and Controls documentation as part of a Drug Master File (DMF) referenced in an Investigative New Drug (IND) application to the FDA. Importantly, our final radiosynthetic procedure is well suited to automation and afforded formulated pure tracer with good yield and SA, despite the need for two reactions steps. Since each step has its own purification and reformulation step, this necessitated implementation of custom-made radiosynthesis equipment in addition to the

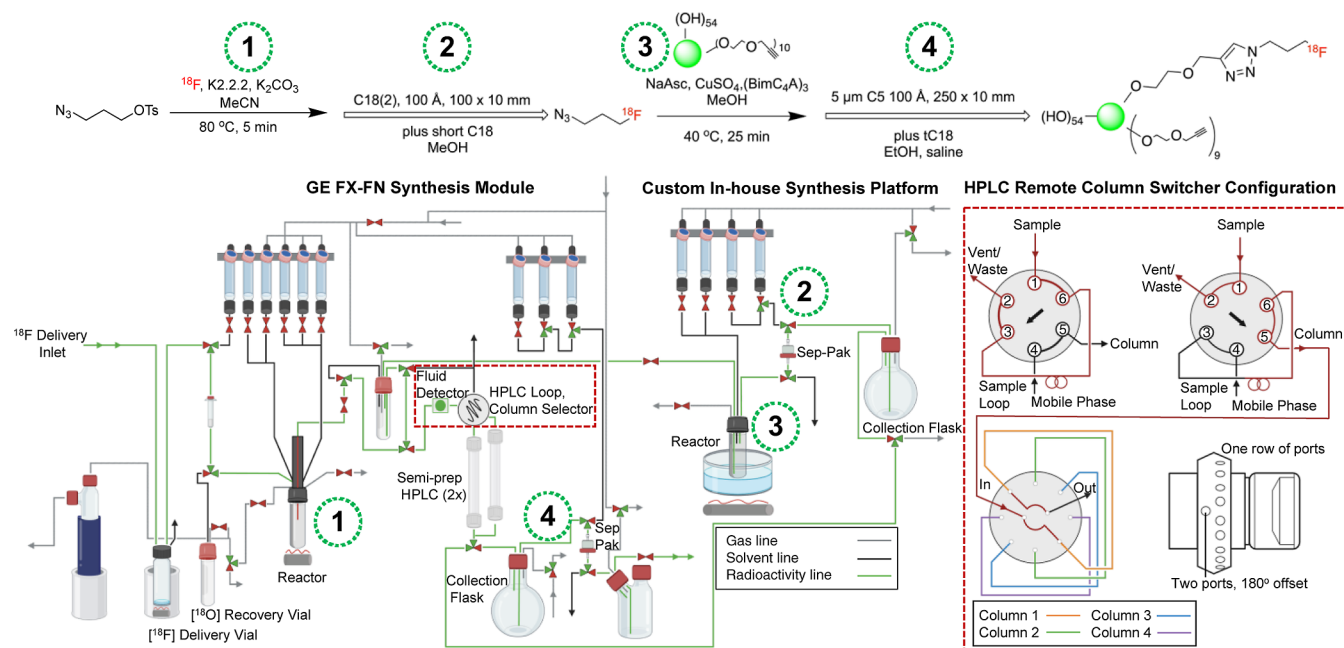


Figure 4. Automated radiosynthesis of [^{18}F]OP-801 for clinical use was performed as follows: (1) [^{18}F]3-Fluoropropylazide was synthesized and purified via HPLC on the FX–FN before. (2) Trapping on a Sep-Pak C-18 plus short on the CM. (3). Elution to a secondary reactor for CuAAC to form crude [^{18}F]OP-801. (4) Crude product was transferred back to the FX–FN, purified via HPLC, and reformulated after trapping on a Sep-Pak tC18 plus to yield pure [^{18}F]OP-801 suitable for human injection.

Table 3. Yield and SA for Validated Clinical [¹⁸F]OP-801 Synthesis

	validation 1	validation 2	validation 3	mean (SD)
starting ¹⁸ F (MBq)	74 629	77 811	93 240	81 893 (9954)
final formulated [¹⁸ F]OP-801 (MBq)	1924.70	2311.02	4240.20	2825.32 (1240.45)
SA (GBq/mg)	32.93	24.79	54.76	37.49 (15.49)
activity yield	2.87%	3.30%	5.06%	3.74% (1.16%)
radiochemical yield	5.12%	6.17%	9.39%	6.89% (2.23%)
total synthesis time (minutes)	92	99	98	96 (3)

FX–FN synthesis module, although an equivalent multi-reactor synthesis platform could be used if available. In our hands, fully automated synthesis was achieved using an FX–FN synthesis module, adjacent custom synthesis platform, and remote control HPLC column selector configured for remote switching between two HPLC columns (Figure 4). The cGMP compliant clinical synthesis was performed consecutively three times to synthesize [¹⁸F]OP-801 with an average of 6.89% (SD 2.23) decay corrected radiochemical yield and 99% radiochemical purity and SA of 37.49 GBq/mg (SD 15.49) (Table 3, Supporting Information Table 3), in approximately 90 min including both steps and reformulation. For all three syntheses, complete QC analysis was performed to meet criteria specified in the approved IND/DMF. All batches successfully passed all QC analyses to confirm purity, identity, sterility, and safety, at both 0 and 4 h after end of synthesis (corresponding to the proposed expiration for clinical grade [¹⁸F]OP-801) and were therefore suitable for human use (Supporting Information Table 4).

2.5. Concluding Remarks. Here, we report the results of multiple IND-enabling experiments as well as the optimization of [¹⁸F]OP-801 radiosynthesis for clinical translation. Taken together, these data combined with our previously reported data highlight the promise of [¹⁸F]OP-801 for clinical imaging of neuroinflammation and also afford valuable lessons in applying volatile reagents and low-precursor-concentration conditions to ¹⁸F click chemistry. The optimized radiosynthesis described here is conducive to reliable production of clinical grade [¹⁸F]OP-801, and the overall optimization process afforded definitive data to support the use of improved approaches to ¹⁸F click chemistry. Successful validation of this radiosynthetic procedure and subsequent FDA authorization to proceed with clinical studies serves as a case study for the utility of our approach for ¹⁸F click chemistry and enables future clinical PET imaging with [¹⁸F]OP-801. A phase 1/2 (NCT05395624) clinical trial is underway for evaluating [¹⁸F]OP-801 in healthy volunteers and ALS patients, underscoring the potential impact of [¹⁸F]OP-801 for imaging reactive microglia and macrophages in clinically relevant neuroinflammatory pathologies. Based on preliminary human imaging data, future work will optimize the synthesis of [¹⁸F]OP-801 for cassette-based radiosynthesis platforms to facilitate widespread use for clinical imaging of neuroinflammation and multi-site studies.

3. MATERIALS AND METHODS

Please see the Supporting Information for detail regarding a single GLP dose toxicology study performed in rats.

3.1. Dosimetry. For all dosimetry studies, [¹⁸F]OP-801 was synthesized via the preclinical synthesis protocol described previously.¹⁴ Radiation-absorbed dose for human subjects was calculated using both *in vivo* imaging of mice in addition to *ex vivo* gamma counting of mouse tissues (see the Supporting Information for detail, Table 5). In both experiments, the total percent injected dose

per gram (% ID/g) associated with each organ was computed. C57BL/6 mice (female *n* = 5; male *n* = 5) were anesthetized using isoflurane in oxygen (2.0–3.5% for induction and 1.0–2.5% for maintenance), and the formulated tracer [¹⁸F]OP-801 (141–232 μCi in saline with 10% ethanol) was administered intravenously via the tail-vein injection. A 60 min dynamic PET scan (Siemens, Inveon D-PET) commenced just prior to tracer administration, and data were acquired in the list mode format. The resulting data were binned and reconstructed into 19 frames (4 × 15s, 4 × 60s, and 11 × 300s). Isotropic resolution was achieved using OSEM3D/MAP reconstruction algorithms with 18 subsets and 2 iterations and a matrix size of 128 × 128 × 159. Static PET images (5 min) were acquired 90 and 240 min post-injection of [¹⁸F]OP-801 (Figure 1). Following all PET scans, CT scans (Sofie, GNEXT PET/CT) were immediately acquired to provide an anatomic reference for the PET data. To ensure accurate co-registration, mice were transferred between scanners in the same bed.

VOIs were hand-drawn over regions of interest (*i.e.*, bone, brain, urinary bladder, heart, kidney, liver, lung, and muscle) using image analysis software (Invivo, VivoQuant) on the CT images for anatomic reference (Supporting Information Figure 1). The total non-decay corrected % ID/g associated with each VOI at each timepoint was calculated for each mouse, then averaged together to arrive at a single non-decay corrected % ID/g associated with each VOI for each time point in male mice and in female mice. This value was converted to % ID/organ for each time point in males and females using a previously described percent kg/g method for animal-to-human biokinetic extrapolation.²⁵ The area under the curve (AUC) was computed for each organ based on % ID/organ; the final timepoint was extrapolated to zero by integrating the exponential radioactive decay function from the 4 h timepoint to infinity. Absorbed doses were calculated using a standard quantitation platform, organ-level internal dose assessment, and bi-exponential model without bladder voiding.

3.2. Radiochemistry, Characterization, and QC Analysis.

3.2.1. General Considerations. All chemicals were acquired from commercial sources and used without further purification unless otherwise stated. Synthetic precursors for fluorination (3-azidopropyl-4-methylbenzenesulfonate) and copper-catalyzed azide–alkyne cycloaddition (CuAAC) [polyamidoamine generation 4 hydroxyl alkyne (10) dendrimer (PAMAM-G4-OH alkyne₁₀)] were synthesized to order by Snapdragon Chemistry and used without further purification.

3.2.2. Radiosynthesis for Clinical Production. The final radiochemistry protocol for synthesis of clinical grade [¹⁸F]OP-801 was reviewed by the Food and Drug Administration (FDA) as a DMF referenced in an IND application. All chemistry was performed on a TRACERlab FX–FN synthesis module (GE) with an adjacent custom synthesis platform (built in-house) and a remote control HPLC column selector (Cheminert 6 port, VICI) (Figure 4). [¹⁸F]fluoride (n.c.a.) in ¹⁸O-water (81 893 ± 9954 MBq) was generated with a GE PETtrace cyclotron via the ¹⁸O(p,n)¹⁸F, passed through a ¹⁸F-PS-HCO₃⁻ separation cartridge (Synthra) (previously conditioned with 1.0 mL of ethanol, 1.0 mL of water, and 1.0 mL of air), and eluted to a glassy carbon reactor with 1.0 mL of a solution containing K₂CO₃ (3.5 mg) and Kryptofix 2.2.2. (15 mg) in MeCN (0.90 mL) and water (0.10 mL). The mixture was heated and dried under vacuum/He at 88 °C for 5 min, followed by cooling to 60 °C. A solution of 3-azidopropyl-4-methylbenzenesulfonate (3.0 ± 0.5 mg) in anhydrous MeCN (1 mL) was added to the reactor and the

solution heated to 80 °C for 5 min, after which the crude reaction mixture was diluted with 2 mL of 0.05 N HCl and purified via semi-preparative HPLC (Supporting Information Table 2). Pure [¹⁸F]3-fluoropropylazide was collected without further dilution (taking care to keep the collected volume <5 mL) and trapped on a Sep-Pak C18 plus short cartridge (Waters) (previously conditioned with 5 mL of ethanol and 10 mL of water).

[¹⁸F]3-Fluoropropylazide was eluted with 1 mL of MeOH into a second reactor containing sodium ascorbate (2.0 mg), copper (II) sulfate (0.25 mg), tripotassium 5,5',5''-[2,2',2''-nitrotris(methylene)-tris(1H-benzimidazole-2,1-diyl)]tripentanoate hydrate [(BIMC4A)3] (0.25 mg), PAMAM-G4-OH alkyne₁₀ dendrimer precursor dissolved in methanol (0.1 mg), and sterile water (50 μL) (Supporting Information Table 1). The reaction mixture was heated to 40 °C for 25 min, diluted with water with 0.1% TFA (3 mL), and purified via semi-preparative HPLC (Supporting Information Table 2). Pure [¹⁸F]OP-801 was diluted with water (25 mL) and passed through a Sep-Pak tC18 plus cartridge (Waters) [previously conditioned with ethanol (5 mL) and water (10 mL)] and washed with sterile water (10 mL), before finally being eluted into a vial with dehydrated ethanol USP (1 mL) and sodium chloride for injection (0.9%) (10 mL). The final solution was passed through a 0.22 μm Millex MP sterile filter (Millipore) to a pre-assembled septum-sealed sterile collection vial (30 mL) for filtration and sterilization. The production of a single unit dose from beginning to release required approximately 1.5 h of elapsed time.

3.2.3. In Vitro Human Plasma Stability. To assess the stability of [¹⁸F]OP-801 in human serum, 2.78 MBq (approx. 20 μL) of formulated [¹⁸F]OP-801 was added to human plasma (330 μL), and the mixture was vortexed briefly. Aliquots (70 μL) were transferred to individual Eppendorf tubes and incubated at 37 °C. Samples were quenched at 0, 5, 15, 30, 60, and 90 min with 140 μL of ice-cold methanol and centrifuged at 12 500g for 10 min. The supernatant was transferred to an HPLC vial and analyzed via HPLC (Agilent 1260 Infinity II) using analytical QC conditions, as described below. Controls consisting of the radiotracer incubated in phosphate-buffered saline without plasma were assessed at 0 and 90 min.

3.2.4. QC Analysis. The FDA stipulates that each batch and dose of clinical grade formulated [¹⁸F]OP-801 must meet all criteria specified in the approved IND/DMF (Supporting Information Table 4) prior to transport to the clinic for administration to humans. To assure [¹⁸F]OP-801 production reliably meets these guidelines, a sample (1.0 mL) of [¹⁸F]OP-801 was removed from the dose vial for QC analysis and clinical validation (*n* = 3), and each batch visually inspected for any coloration or particulate. MColorpHast pH strips (EMD, Millipore) were used to determine the pH of the final product. (Radio)-Chemical purity and identity were analyzed via analytical HPLC, as previously described (Supporting Information Figure 2, Table 2). A standard calibration curve was generated using [¹⁹F]OP-801 and used to determine the total carrier mass of non-radioactive [¹⁸F]OP-801 and derivatives as well as the SA for each batch. Radio-nuclidic identity and purity were determined using a dose calibrator (Capintec) and gamma ray multi-channel analyzer (MCA) (ASA-11 NaI MCA, Canberra), respectively. Residual solvent analysis was carried out using gas chromatography (6850 series, Agilent) with a DB-Wax Capillary column (30 m × 0.25 mm × 0.25 μm) (Agilent). Apyrogenicity tests (Charles River Laboratories, Inc., USA) were performed to ensure that all doses of [¹⁸F]OP-801 contained <175 endotoxin units per batch. A bubble-point testing device (custom, in-house) was assembled and used to assess filter integrity of the sterile filter used to sterilize final formulated [¹⁸F]OP-801. Sterility testing was performed in-house by the Molecular Imaging Program at Stanford (MIPS) Cyclotron and Radiochemistry Facility (CRF). For clinical validation runs (*n* = 3), all QC analysis was performed at 0 and 4 h after end of synthesis (EOS) for each batch, corresponding to an expiration date of 4 h after EOS.

■ ASSOCIATED CONTENT

📄 Supporting Information

The Supporting Information is available free of charge at <https://pubs.acs.org/doi/10.1021/acschemneuro.3c00028>.

Additional experimental details, materials and methods, and results regarding toxicology studies, dosimetry predictions, and synthesis and characterization of clinical grade [¹⁸F]OP-801 (PDF)

■ AUTHOR INFORMATION

Corresponding Author

Michelle L. James – Stanford University Department of Radiology, Stanford, California 94305, United States; Stanford University Department of Neurology and Neurological Sciences, Stanford, California 94305, United States; Phone: 650-497-0153; Email: mljames@stanford.edu

Authors

Isaac M. Jackson – Stanford University Department of Radiology, Stanford, California 94305, United States; orcid.org/0000-0002-6928-7551
Mackenzie L. Carlson – Stanford University Department of Bioengineering, Stanford, California 94305, United States
Corinne Beinat – Stanford University Department of Radiology, Stanford, California 94305, United States
Noeen Malik – Stanford University Department of Radiology, Stanford, California 94305, United States
Mausam Kalita – Stanford University Department of Radiology, Stanford, California 94305, United States
Samantha Reyes – Stanford University Department of Radiology, Stanford, California 94305, United States
E. Carmen Azevedo – Stanford University Department of Radiology, Stanford, California 94305, United States; orcid.org/0000-0002-3942-6979
Sydney C. Nagy – Stanford University Department of Radiology, Stanford, California 94305, United States
Israt S. Alam – Stanford University Department of Radiology, Stanford, California 94305, United States
Rishi Sharma – Ashvattha Therapeutics, Inc., Redwood City, California 94065, United States
Santiago Appiani La Rosa – Ashvattha Therapeutics, Inc., Redwood City, California 94065, United States
Farshad Moradi – Stanford University Department of Radiology, Stanford, California 94305, United States
Jeffrey Cleland – Ashvattha Therapeutics, Inc., Redwood City, California 94065, United States
Bin Shen – Stanford University Department of Radiology, Stanford, California 94305, United States

Complete contact information is available at:

<https://pubs.acs.org/10.1021/acschemneuro.3c00028>

Author Contributions

I.M.J. and M.L.C. contributed equally to this work. I.M.J.: radiochemistry conceptualization/troubleshooting/optimization, methodology, investigation and analysis, writing original draft, and creating tables and figures. M.L.C.: conceptualization, methodology, dosimetry and imaging investigation, formal analysis, writing original draft, and creating tables and figures. C.B.: dosimetry study design, investigation and analysis, manuscript review, and editing. N.M.: radiochemistry conceptualization/troubleshooting/optimization, methodol-

ogy, investigation and analysis, manuscript review, and editing. M.K. and R.S.: radiochemistry conceptualization, methodology, manuscript review, and editing. S.R., E.C.A., S.C.N., and I.S.A.: dosimetry investigation, manuscript review, and editing. F.M.: supervision, data interpretation, guidance on clinical translation, manuscript review, and editing. S.A.L.R.: dendrimer development, synthesis, conceptualization, and methodology. J.C.: supervision, study design, funding acquisition, manuscript review, and editing. B.S.: radiochemistry conceptualization/troubleshooting/optimization, methodology, investigation, supervision, manuscript writing, and editing. M.L.J.: conceptualization, study design, data interpretation, manuscript writing, editing, supervision, and funding acquisition.

Funding

The authors would like to acknowledge Ashvattha Therapeutics and NSF GRFP grant number: DGE—1656518 for funding. I.M.J. was supported by the Stanford University Medical Scientist Training Program (grant T32-GM007365 and T32-GM145402).

Notes

The authors declare the following competing financial interest(s): R.S., S.A.L., and J.C. were employed by Ashvattha Therapeutics during the completion of this work.

REFERENCES

- (1) Zürcher, N. R.; Loggia, M. L.; Lawson, R.; Chonde, D. B.; Izquierdo-Garcia, D.; Yasek, J. E.; Akeju, O.; Catana, C.; Rosen, B. R.; Cudkovic, M. E.; Hooker, J. M.; Atassi, N. Increased in Vivo Glial Activation in Patients with Amyotrophic Lateral Sclerosis: Assessed with [11C]-PBR28. *NeuroImage Clin.* **2015**, *7*, 409–414.
- (2) Hanisch, U.-K.; Kettenmann, H. Microglia: Active Sensor and Versatile Effector Cells in the Normal and Pathologic Brain. *Nat. Neurosci.* **2007**, *10*, 1387–1394.
- (3) Werry, E. L.; Bright, F. M.; Piguet, O.; Ittner, L. M.; Halliday, G. M.; Hodges, J. R.; Kiernan, M. C.; Loy, C. T.; Kril, J. J.; Kassiu, M. Recent Developments in TSPO PET Imaging as a Biomarker of Neuroinflammation in Neurodegenerative Disorders. *Int. J. Mol. Sci.* **2019**, *20*, No. E3161.
- (4) Owen, D. R.; Yeo, A. J.; Gunn, R. N.; Song, K.; Wadsworth, G.; Lewis, A.; Rhodes, C.; Pulford, D. J.; Bennacef, I.; Parker, C. A.; StJean, P. L.; Cardon, L. R.; Mooser, V. E.; Matthews, P. M.; Rabiner, E. A.; Rubio, J. P. An 18-KDa Translocator Protein (TSPO) Polymorphism Explains Differences in Binding Affinity of the PET Radioligand PBR28. *J. Cereb. Blood Flow Metab.* **2012**, *32*, 1–5.
- (5) Horti, A. G.; Naik, R.; Foss, C. A.; Minn, I.; Mishneva, V.; Du, Y.; Wang, Y.; Mathews, W. B.; Wu, Y.; Hall, A.; LaCourse, C.; Ahn, H.-H.; Nam, H.; Lesniak, W. G.; Valentine, H.; Pletnikova, O.; Troncoso, J. C.; Smith, M. D.; Calabresi, P. A.; Savonenko, A. V.; Dannals, R. F.; Pletnikov, M. V.; Pomper, M. G. PET Imaging of Microglia by Targeting Macrophage Colony-Stimulating Factor 1 Receptor (CSF1R). *Proc. Natl. Acad. Sci. U.S.A.* **2019**, *116*, 1686–1691.
- (6) Tewari, M.; Seth, P. Emerging Role of P2X7 Receptors in CNS Health and Disease. *Ageing Res. Rev.* **2015**, *24*, 328–342.
- (7) Nance, E.; Zhang, F.; Mishra, M. K.; Zhang, Z.; Kambhampati, S. P.; Kannan, R. M.; Kannan, S. Nanoscale Effects in Dendrimer-Mediated Targeting of Neuroinflammation. *Biomaterials* **2016**, *101*, 96–107.
- (8) Perumal, O. P.; Inapagolla, R.; Kannan, S.; Kannan, R. M. The Effect of Surface Functionality on Cellular Trafficking of Dendrimers. *Biomaterials* **2008**, *29*, 3469–3476.
- (9) Tunki, L.; Kulhari, H.; Bhargava, S. K.; Pooja, D. 4 - Pharmacokinetic Considerations in Design of Dendrimer-Based Nanomedicines. In *Pharmaceutical Applications of Dendrimers*; Chauhan, A., Kulhari, H., Eds.; Elsevier, 2020, pp 93–106. Micro and Nano Technologies
- (10) Seo, J. W.; Baek, H.; Mahakian, L. M.; Kusunose, J.; Hamzah, J.; Ruoslahti, E.; Ferrara, K. W. 64Cu-Labeled LyP-1-Dendrimer for PET-CT Imaging of Atherosclerotic Plaque. *Bioconjugate Chem.* **2014**, *25*, 231–239.
- (11) Xiao, T.; Li, D.; Shi, X.; Shen, M. PAMAM Dendrimer-Based Nanodevices for Nuclear Medicine Applications. *Macromol. Biosci.* **2020**, *20*, No. e1900282.
- (12) Trembleau, L.; Simpson, M.; Cheyne, R. W.; Escofet, I.; Appleyard, M. V. C. A. L.; Murray, K.; Sharp, S.; Thompson, A. M.; Smith, T. A. D. Development of 18F-Fluorinatable Dendrons and Their Application to Cancer Cell Targeting. *New J. Chem.* **2011**, *35*, 2496–2502.
- (13) Zhao, L.; Shi, X.; Zhao, J. Dendrimer-Based Contrast Agents for PET Imaging. *Drug Delivery* **2017**, *24*, 81–93.
- (14) Carlson, M.; Azevedo, E. C.; Kellow, R.; Reyes, S.; Alam, I.; Castillo, J.; Shen, B.; Lacor, P.; Sharma, R.; Brewer, M.; Cleland, J.; James, M.; Press, 2023. Synthesis and Characterization of a Novel Hydroxyl Dendrimer-Based PET Tracer for Imaging Maladaptive Neuroinflammation, 18F-OP-801, and Evaluation in a Mouse Model of Lipopolysaccharide-Induced Sepsis
- (15) Alnasser, Y.; Kambhampati, S. P.; Nance, E.; Rajbhandari, L.; Shrestha, S.; Venkatesan, A.; Kannan, R. M.; Kannan, S. Preferential and Increased Uptake of Hydroxyl-Terminated PAMAM Dendrimers by Activated Microglia in Rabbit Brain Mixed Glial Culture. *Molecules* **2018**, *23*, No. E1025.
- (16) Henningfield, C. M.; Cleland, J. L.; Sharma, R.; Green, K. N. Selective Targeting of Plaque-Associated Microglia through Systemic Dendrimer Administration in an Alzheimer's Disease Model. *Alzheimers Dement.* **2020**, *16*, No. e040661.
- (17) Carlson, M.; Jackson, I.; Alam, I.; Kalita, M.; Beiant, C.; Acosta, C.; Falk, I.; Reyes, S.; Nagy, S.; Azevedo, E. C.; Le Moan, N.; Sharma, R.; Cleland, J.; Shen, B.; James, M. Specific Detection of Pathogenic Myeloid Cells in a Mouse Model of Multiple Sclerosis Using [18F]OP-801 before and after Treatment with a CSF1R Inhibitor. *Mol. Imaging Biol.* **2022**, *24*, 63–480.
- (18) Guidance for Industry. M3(r2) Nonclinical Safety Guides for the Conduct of Human Clinical, Trials and Marketing Authorization for Pharmaceuticals. <https://www.fda.gov/regulatory-information/search-fda-guidance-documents/m3r2-nonclinical-safety-studies-conduct-human-clinical-trials-and-marketing-authorization> (accessed Nov 20, 2022).
- (19) Kesner, A. L.; Hsueh, W.-A.; Czernin, J.; Padgett, H.; Phelps, M. E.; Silverman, D. H. S. Radiation Dose Estimates for [18F]5-Fluorouracil Derived from PET-Based and Tissue-Based Methods in Rats. *Mol. Imaging Biol.* **2008**, *10*, 341–348.
- (20) Cicone, F.; Gnesin, S.; Denoël, T.; Stora, T.; van der Meulen, N. P.; Müller, C.; Vermeulen, C.; Benešová, M.; Köster, U.; Johnston, K.; Amato, E.; Auditore, L.; Coukos, G.; Stabin, M.; Schaefer, N.; Viertel, D.; Prior, J. O. Internal Radiation Dosimetry of a 152Tb-Labeled Antibody in Tumor-Bearing Mice. *EJNMMI Res.* **2019**, *9*, 53.
- (21) CFR - Code of Federal Regulations Title 21. <https://www.accessdata.fda.gov/scripts/cdrh/cfdocs/cfcfr/CFRSearch.cfm?CFRPart=361> (accessed Nov 20, 2022).
- (22) Liaw, K.; Zhang, F.; Mangraviti, A.; Kannan, S.; Tyler, B.; Kannan, R. M. Dendrimer size effects on the selective brain tumor targeting in orthotopic tumor models upon systemic administration. *Bioeng. Transl. Med.* **2020**, *5*, No. e10160.
- (23) Mishra, M. K.; Beaty, C. A.; Lesniak, W. G.; Kambhampati, S. P.; Zhang, F.; Wilson, M. A.; Blue, M. E.; Troncoso, J. C.; Kannan, S.; Johnston, M. V.; Baumgartner, W. A.; Kannan, R. M. Dendrimer Brain Uptake and Targeted Therapy for Brain Injury in a Large Animal Model of Hypothermic Circulatory Arrest. *ACS Nano* **2014**, *8*, 2134–2147.
- (24) Lesniak, W. G.; Mishra, M. K.; Jyoti, A.; Balakrishnan, B.; Zhang, F.; Nance, E.; Romero, R.; Kannan, S.; Kannan, R. M. Biodistribution of Fluorescently Labeled PAMAM Dendrimers in

Neonatal Rabbits: Effect of Neuroinflammation. *Mol. Pharmaceutics* **2013**, *10*, 4560–4571.

(25) Kirschner, A.; Ice, R.; Beierwaltes, W. Radiation Dosimetry of ¹³¹I-19-Iodocholesterol: The Pitfalls of Using Tissue Concentration Data-Reply. *J. Nucl. Med.* **1975**, *16*, 248–249.